Article

Mn₃O₄/NiO Nanoparticles Decorated on Carbon Nanofibers as an Enzyme-Free Electrochemical Sensor for Glucose Detection

Mengjie Li [1], Jie Dong [1], Dongmei Deng [1,*], Xun Ouyang [1], Xiaoxia Yan [1], Shima Liu [2] and Liqiang Luo [1,*]

1   College of Sciences, Shanghai University, Shanghai 200444, China
2   Key Laboratory of Hunan Forest Products and Chemical Industry Engineering, Jishou University, Jishou 416000, China
*   Correspondence: dmdeng@shu.edu.cn (D.D.); luck@shu.edu.cn (L.L.); Tel.: +86-21-66132404 (L.L.)

Abstract: Transition metal oxides have garnered a lot of attention in the field of electrocatalysis along with their unique crystal structure and excellent catalytic properties. In this study, carbon nanofibers (CNFs) decorated with Mn_3O_4/NiO nanoparticles were made using electrospinning and calcination. The conductive network constructed by CNFs not only facilitates electron transport, but also provides landing sites for nanoparticles, thus reducing nanoparticle aggregation and exposing more active sites. Additionally, the synergistic interaction between Mn_3O_4 and NiO improved electrocatalytic capacity for glucose oxidation. The Mn_3O_4/NiO/CNFs modified glassy carbon electrode shows satisfactory results in terms of linear range and anti-interference capability for glucose detection, suggesting that the constructed enzyme-free sensor has a promising application in clinical diagnosis.

Keywords: electrospinning; Mn_3O_4/NiO nanoparticles; carbon nanofibers; glucose biosensor

1. Introduction

Electrochemical glucose sensors perform an indispensable role in monitoring glucose concentrations, which not only can be employed to control the intake of glucose in diet, but also to predict diseases associated with high or low glucose levels [1,2]. Enzyme-based sensors show excellent sensitivity and accuracy for glucose detection, but they are sensitive to temperature and pH which limits their storage and transportation [3]. In contrast, enzyme-free sensors have the advantage of being cheap, stable, and sensitive [4], thus attracting considerable attention in recent years.

Noble metals and their alloys have shown excellent catalytic properties and stability [5,6] and are often used as enzyme-free sensors for glucose detection [7,8]. However, the high cost and scarcity of resources limit wide applications of noble metals. In this regard, transition metal can overcome the drawbacks mentioned above for noble metals and be applied as catalysts for many reactions [9], such as CO_2 utilization [10], oxygen evolution reaction [11], and oxygen reduction reaction [12,13]. Generally speaking, composite transition metal oxides exhibit higher catalytic capacity and lower catalytic potential than single transition metal oxide due to the synergistic effect between different metal oxides. Wang et al. synthesized $CuCo_2O_4$/NiO nanoneedle arrays, modified on carbon cloth by hydrothermal method, which were used as self-supporting electrodes for the glucose detection [14]. Xu et al. fabricated CuO-NiO nanocomposites for the detection of glucose which exhibited excellent selectivity, reproducibility, and long-time stability [15].

One-dimensional nanofibers possess low density, large aspect ratio, and high charge carrier directed mobility [16]. Thomas et al. grew α-MoO_3 nanorods on glass substrates by thermal evaporation for ammonia sensing at room temperature [17]. Zhang et al. used a hydrothermal method with low temperature growth to synthesize Co_9S_8 nanotubes @CuS nanosheets, which were modified on glassy carbon electrode (GCE) for the detection of glucose and H_2O_2 [18]. Kokulnathan et al. synthesized TiO/Au nanofibers by electrospinning for the determination of diphenylamine in food [19]. Among the above methods,

electrospinning is a simple, efficient, and inexpensive way to synthesize one-dimensional nanofibers [16,20]. Transition metal oxides/carbon nanofibers composites fabricated by electrospinning have the following advantages: (i) CNFs with large aspect ratio can form a conductive network, which facilitates the electron transport [21]; (ii) the mesh structure can serve as a substrate to support the nanoparticles which allows more active sites of the nanoparticles to be exposed; and, (iii) the synergistic interaction between transition metal oxides and carbon nanofibers can facilitate the electrocatalytic performance.

In this study, CNFs decorated with Mn_3O_4/NiO nanoparticles (Mn_3O_4/NiO/CNFs) were synthesized using electrospinning and subsequent heat treatment. The presence of CNFs not only increases the conductivity of the material, but also expands the active surface area of the catalysts. Additionally, the multivalence of transition metals facilitates the redox reaction at the electrode surface. The synergistic effect between Mn_3O_4 and NiO is beneficial to improve the catalytic performance of glucose oxidation. It is worth noting that the constructed sensor has a good range of linearity, low detection limit, and outstanding interference immunity, indicating that the constructed enzyme-free sensor is promising in clinical diagnosis.

## 2. Experimental Section

2.1. Materials

Polyacrylonitrile (PAN) was supplied by Sigma-Aldrich (St. Louis, MO, USA). $Mn(Ac)_2 \cdot 4H_2O$, N,N-dimethylformamide (DMF), NaOH, glycocoll (Gly), $Ni(Ac)_2 \cdot 4H_2O$, and glucose (Glu) were supported by Sinopharm Chemical Reagent Co., Ltd. (Shanghai, China). Sucrose (Suc), dopamine (DA), maltose (Mal), ascorbic acid (AA), fructose (Fru), uric acid (UA), and NaCl were bought from Alfa Aesar Co., Ltd. (Shanghai, China). Millipore water (18.25 MΩ cm) was used.

2.2. Instrumentations

The scanning electron microscope (SEM, SU5000, HITACHI, Tokyo, Japan) was utilized to observe the morphology and size of materials. The high-resolution transmission electron microscope (HRTEM; JEM 2100F, JEOL, Tokyo, Japan) was further used to investigate the microscopic crystal structure of samples. X-ray diffraction (XRD, D/MAX2200, Rigaku, Tokyo, Japan) was employed to characterize the crystal structure of the materials. Fourier transform infrared spectroscopy (FTIR, AVATAR370, Thermo Scientific, Waltham, MA, USA) was performed to study chemical structure. The degree of graphitization of CNFs was studied by Raman spectrum (INVIA, Renishaw, London, UK). X-ray photoelectron spectrometer (XPS, ESCALAB-250XI, Thermo Scientific, Waltham, MA, USA) was applied to measure the surface components of materials in qualitative detail.

2.3. Synthesis of Mn_3O_4/NiO/CNFs

The synthesis process of Mn_3O_4/NiO/CNFs is illustrated in Scheme 1. Firstly, 0.5 g of PAN was mixed with 10 mL DMF and agitated to form a transparent solution. Then, 0.068 g $Mn(Ac)_2 \cdot 4H_2O$ and 0.017 g $Ni(Ac)_2 \cdot 4H_2O$ were added to the above solution and stirred continuously. Afterwards, the obtained brown precursor solution was moved to a 10 mL plastic injection syringe, and delivered to the metal needle at a constant stream rate of 0.6 mL h^{-1} under control of an injection pump. The grounded aluminum plate was used as the collector and kept away from the needle at a distance of 12 cm. After electrospinning, the collected precursor fibers were dried overnight at 60 °C under vacuum. The dried precursor fibers were pre-oxidized in air at 250 °C for 2 h, and then carbonized at 800 °C for another 2 h in an Ar stream. For comparison, Mn_3O_4/CNFs and NiO/CNFs were synthesized by the same method.
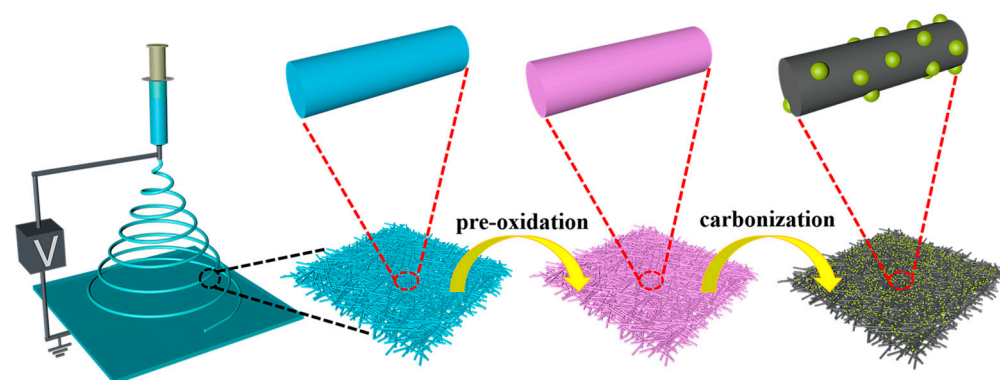
Scheme 1. Schematic diagram of synthesis procedure of Mn_3O_4/NiO/CNFs.

2.4. Electrochemical Measurements

The electrochemical measurements were carried out in a three-electrode system consisting of a platinum wire as counter electrode, Ag/AgCl (saturated KCl) as reference electrode, and Mn_3O_4/NiO/CNFs/GCE as working electrode. The three-electrode system was connected to an electrochemical workstation (CHI 842D, CH Instruments, Shanghai, China). The Mn_3O_4/NiO/CNFs/GCE was prepared in following steps: the bare GCE was polished with aluminum powder (0.5 μm and 0.01 μm), followed by cleaning with deionized water. Then, 5 μL of Mn_3O_4/NiO/CNFs uniform dispersion was dropped on GCE and then dried under infrared light to obtain Mn_3O_4/NiO/CNFs/GCE for glucose detection. The supporting electrolyte was 0.1 M NaOH.

3. Results and Discussion

3.1. XRD, Raman, FT-IR, and XPS Characterization of Mn_3O_4/NiO/CNFs

The crystal structure and purity of Mn_3O_4/NiO/CNFs were characterized with XRD. Figure 1a shows the XRD patterns of Mn_3O_4/CNF, NiO/CNF, and Mn_3O_4/NiO/CNF. The obtained material contained a set of diffraction peaks that matched with Mn_3O_4, NiO, and CNF. In addition, there were no other impure phases. The peak at 24.2° could be ascribed to the (200) plane of CNF. The diffraction peaks at 37.2°, 43.2°, 62.8°, and 75.4° displayed the crystal planes of (111), (200), (220), and (311) plane for NiO [22]. The diffraction peaks at 17.9°, 28.9°, 31.0°, 32.3°, 36.1°, 38.0°, 44.4°, 50.7°, 53.1°, 56.0°, 58.5°, 59.9°, and 64.5° were well indexed to the (101), (112), (200), (103), (211), (004), (220), (105), (312), (303), (321), (224), and (400) plane of Mn_3O_4 with a cubic spinel [23].
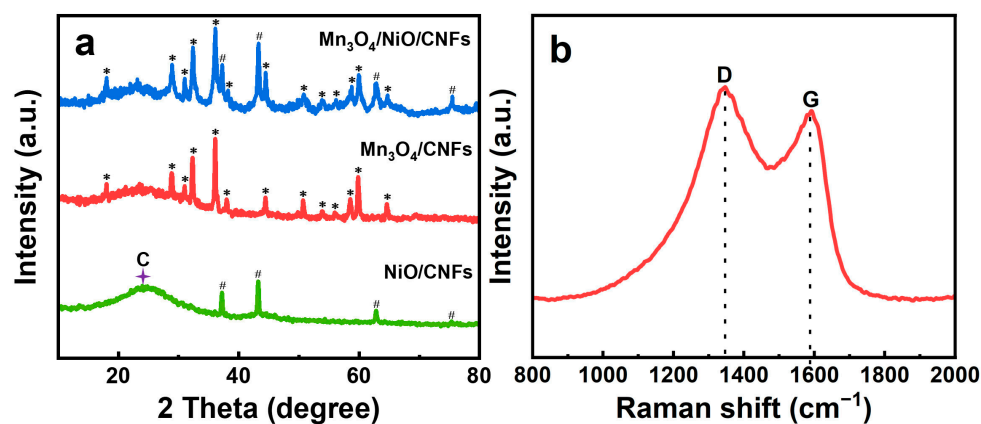

Figure 1. (**a**) XRD patterns of Mn_3O_4/CNFs, NiO/CNFs, and Mn_3O_4/NiO/CNFs; (**b**) Raman spectrum of Mn_3O_4/NiO/CNFs at 800 °C.

The Raman spectrum was applied to evaluate the degree of graphitization of CNFs. In Figure 1b, the Raman spectrum shows a couple of significant peaks at 1350 and 1590 cm^{-1}

which were directly related to the D band and G band, respectively [24]. The intensity of the D band reflected the carbon defects, while the intensity of the G band gave information about the graphitic structure. The intensity ratio between the D and G band, $R = I_D/I_G$, can be used to reflect the degree of graphitization of CNFs [25]. The R value is 1.07, which means that there are still defects in the material under calcination at 800 °C. The explanation for the defect is that the N element in PAN has not been completely removed. As shown in Figure S1, an FT-IR spectrum of $Mn_3O_4/NiO/CNFs$ was performed. The band at 3444 cm^{-1} is identified as the stretching vibration of O-H, which is related to the adsorption of water. The peak at 1620 cm^{-1} can correspond to the C=C bond. The weak peak observed at 1383 cm^{-1} can be attributed to the C-H bond. The band at about 1169 cm^{-1} is caused by C-O [26]. The peaks which appear at 618 cm^{-1} and 523 cm^{-1} can be traced back to Mn_3O_4 and NiO, respectively [27].

The elemental composition and valence state of the $Mn_3O_4/NiO/CNFs$ were reflected using XPS technique. The fully scanned spectrum (Figure 2a) demonstrates that the synthesized materials contained elements of C, N, O, Ni, and Mn. The peaks located at 854.7 eV and 872.1 eV were associated with Ni $2p_{3/2}$ and Ni $2p_{1/2}$, which were derived from Ni^{2+} (Figure 2b). In addition, two satellite peaks accompanying the main peaks were observed at 861.5 eV and 879.8 eV, proving the presence of Ni^{2+} from NiO [28]. The peaks located at 856.5 eV and 874.0 eV in Ni 2p spectrum corresponded to Ni $2p_{3/2}$ and Ni $2p_{1/2}$ from Ni^{3+}, respectively. Here, more energy was required to form Ni^{3+} than Ni^{2+}, since the compensation of large amounts of charge leads to the introduction of Ni vacancies and oxygen gaps, which in turn cause the formation of Ni^{3+} [29,30]. As shown in Figure 2c, the Mn 2p spectrum consists of a pair of major peaks located at 653.3 eV and 641.6 eV. The deconvolution peaks at the binding energies of 640.9 eV/652.4 eV and 642.3 eV/653.7 eV were caused by Mn^{2+} and Mn^{3+} species, respectively. The peaks located at about 645.0 eV and 655.0 eV belong to satellite peaks. Four peaks with energies of 284.6 eV, 285.6 eV, 287.4 eV, and 290.1 eV, corresponding to C=C, C-C, C=O/C=N, and O=C-O bonds, respectively, were fitted from the high-resolution C 1s peak (Figure 2d) [31,32]. The O 1s spectrum can be divided into three characteristic peaks, where the peaks of T-O-T and T-OH (T symbolizes transition metal) were observed at 529.9 eV and 531.2 eV, respectively. Moreover, the binding energy value of O 1s located at 533.2 eV represents the water-adsorbed on the surface (H-O-H) (Figure 2e). In the spectrogram of N 1s (Figure 2f), three peaks located at 398.8 eV, 400.1 eV, and 402.0 eV can be considered as pyridinic N, pyrrolic N, and graphitic N, respectively. Among them, pyridinic N and pyrrolic N are the two main doping forms in CNF [33].
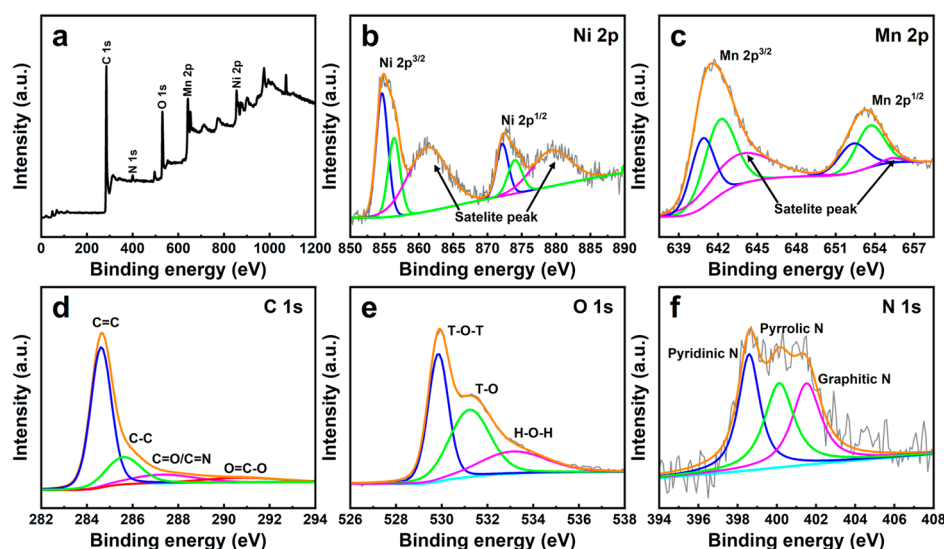

Figure 2. XPS spectra of $Mn_3O_4/NiO/CNFs$: (**a**) full wide-scan; (**b**) Ni 2p; (**c**) Mn 2p; (**d**) C 1s; (**e**) O 1s; and (**f**) N 1s.

3.2. SEM and TEM of Mn₃O₄/NiO/CNFs

The surface morphologies of $Mn(Ac)_2/Ni(Ac)_2/PAN$ precursor nanofibers and $Mn_3O_4/NiO/CNFs$ were observed through SEM. In Figure 3a, the surface of uncalcined precursor nanofibers was smooth due to the amorphous structure of $Ni(Ac)_2$ and $Mn(Ac)_2$. After calcination at 800 °C, the nanoparticles were uniformly dispersed on the nanofiber surface (Figure 3b). The previous XRD result confirmed that the nanoparticle consisted of Mn_3O_4 and NiO. The diameter statistics and Gaussian distribution of the precursor nanofibers and $Mn_3O_4/NiO/CNFs$ are shown in the insets of Figure 3a,b. Obviously, the average diameter of the nanofibers decreased from 168 to 115 nm after calcination, a phenomenon which was ascribed to the reduction of huge amount of H, O, and N elements during the carbonization process. TEM and HRTEM were carried out to further reveal the microscopic crystal structure of $Mn_3O_4/NiO/CNF$. As shown in Figure 3c, Mn_3O_4/NiO nanoparticles were uniformly adhered to the CNF surface. Lattice fringes with spacing of 0.308 nm and 0.289 nm corresponds to the (112) plane of Mn_3O_4 and (200) plane of NiO, respectively (Figure 3d) [34,35].
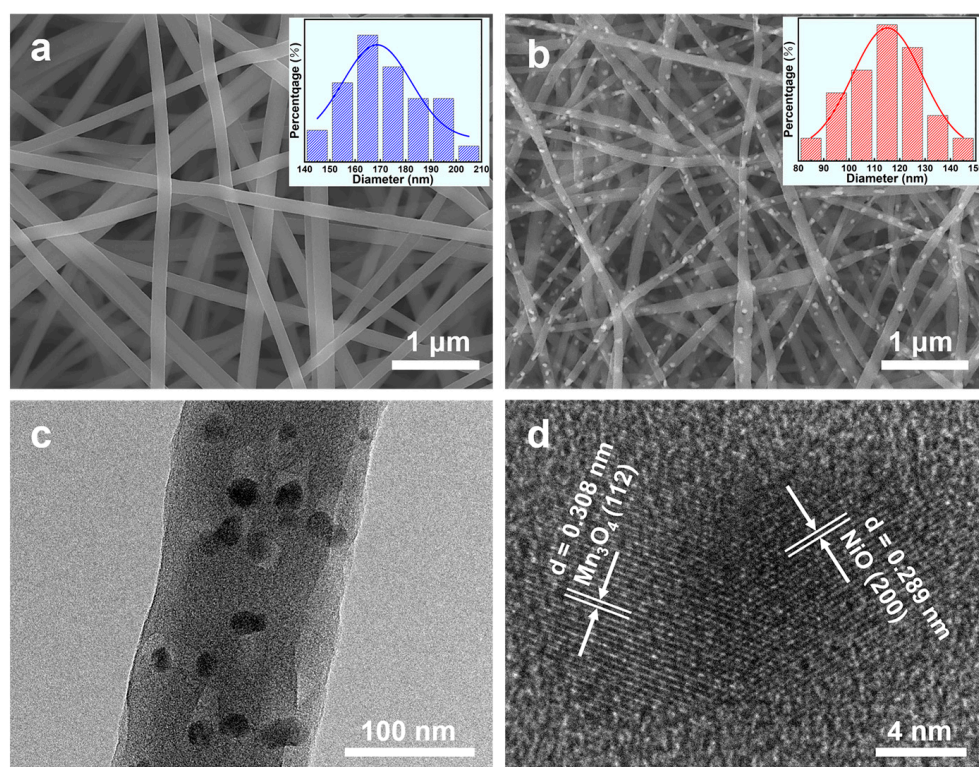

Figure 3. SEM images of electrospun: (**a**) $Mn(Ac)_2/Ni(Ac)_2/PAN$ nanofibers and (**b**) $Mn_3O_4/NiO/$ CNFs; (**c**) TEM image of $Mn_3O_4/NiO/CNFs$; (**d**) HRTEM image of Mn_3O_4/NiO.

3.3. Electrochemical Characterization

The cyclic voltammetry (CV) and electrochemical impedance spectroscopy (EIS) were used to study the electrochemical performance of $Mn_3O_4/NiO/CNFs$. EIS tests of different modified electrodes were conducted in the solution with 5 mM $[Fe(CN)_6]^{3-/4-}$ and 0.1 M KCl. The outcome of the EIS test is reflected by the Nyquist plot, where the semicircular part of the high frequency region relates to the electron transfer restriction process and the linear part of the low frequency region reflects the diffusion process. The decrease in the radius of the semicircle represents a decrease in the electron transfer resistance at the electrode interface (R_{et}). In Figure S2, compared to $Mn_3O_4/CNFs/GCE$ and $NiO/CNFs/GCE$, $Mn_3O_4/NiO/CNFs/GCE$ shows the smallest diameter, indicating the fastest charge transfer capability. To investigate the electrochemical performance of $Mn_3O_4/NiO/CNFs$, CV was employed. Figure 4a shows the CV curves of $Mn_3O_4/CNFs/GCE$, $NiO/CNFs/GCE$,

and $Mn_3O_4/NiO/CNFs/GCE$ in 0.1 M NaOH solution with and without 2 mM glucose. The oxidation current that changed for $Mn_3O_4/CNFs/GCE$ in the presence of glucose can be neglected. Meanwhile, $NiO/CNFs/GCE$ exhibited a positive electrocatalytic oxidation peak current for glucose detection which can be ascribed to the transition between Ni^{2+} and Ni^{3+}. Notably, $Mn_3O_4/NiO/CNFs/GCE$ exhibited the highest oxidation current. The mechanism of glucose oxidation on $Mn_3O_4/NiO/CNFs$ can be explained by the following equations [36]:
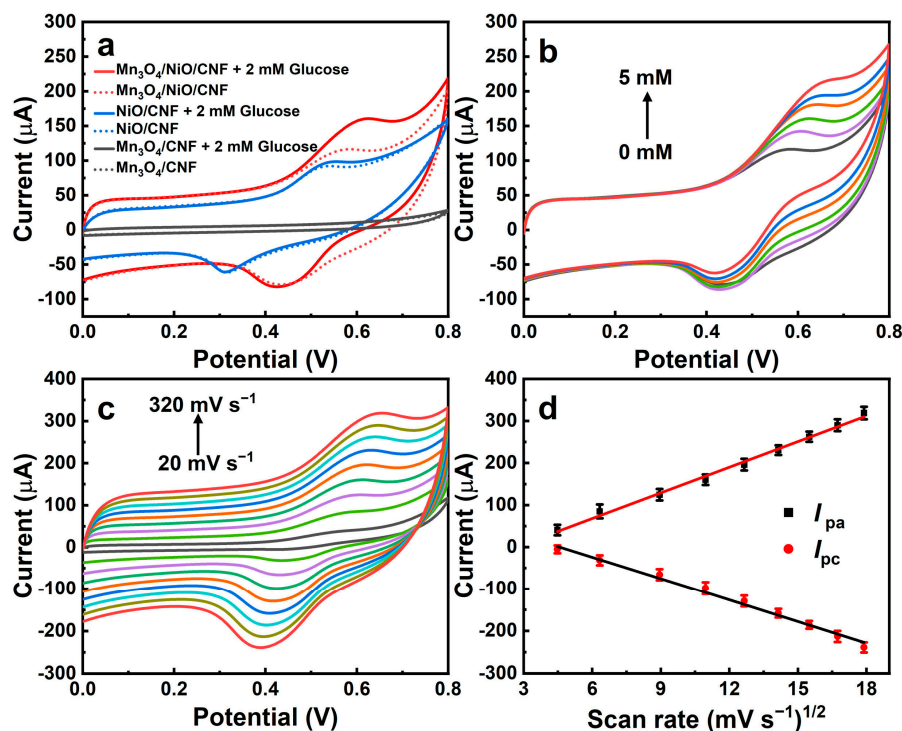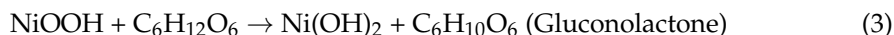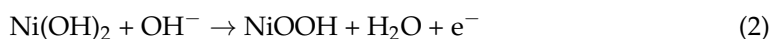
$$NiO + H_2O \rightarrow Ni(OH)_2 \tag{1}$$

$$Ni(OH)_2 + OH^- \rightarrow NiOOH + H_2O + e^- \tag{2}$$

$$NiOOH + C_6H_{12}O_6 \rightarrow Ni(OH)_2 + C_6H_{10}O_6 \; (Gluconolactone) \tag{3}$$

Figure 4. (**a**) CVs of $Mn_3O_4/CNFs$, $NiO/CNFs$, and $Mn_3O_4/NiO/CNFs$ electrodes in the absence and presence of 2 mM glucose; (**b**) CVs of $Mn_3O_4/NiO/CNFs$ electrode with different concentrations of glucose in 0.1 M NaOH at the scan rate of 100 mV s^{-1}; (**c**) CVs of $Mn_3O_4/NiO/CNFs$ electrode in the presence of 1 mM glucose at different scan rates; (**d**) peak currents in relationship to the square root of the scanning speed scan rate.

Originally, in the alkaline medium, NiO strongly adsorbed water molecules to form $Ni(OH)_2$ (Equation (1)). Next, $Ni(OH)_2$ was oxidized to NiOOH as electron mediator (Equation (2)). Then, NiOOH obtained electrons from glucose to form $Ni(OH)_2$, and glucose was oxidized to gluconolactone (Equation (3)). Previous studies have indicated that Mn-based materials have a wide range for enzyme-free detection of glucose [37,38]. In this work, by virtue of the synergistic interaction between Mn and Ni, the composite exhibits more significant electrocatalytic activity for the oxidation of glucose [39]. The results of the EIS also confirm that the introduction of Mn_3O_4 can increase the electrical conductivity of the composites.

Figure 4b describes the CV curves of $Mn_3O_4/NiO/CNFs/GCE$ in different glucose concentrations (from 0 mM to 5 mM). The oxidation current signal increased with increasing glucose concentration, indicating that $Mn_3O_4/NiO/CNFs$ are suitable as electrocatalytic media for the construction of glucose sensors. To further investigate the kinetic process of glucose oxidation on the electrode surface, the CV curves of $Mn_3O_4/NiO/CNFs/GCE$ were

tested in the range of scan rate from 20 mV s^{-1} to 320 mV s^{-1} (Figure 4c). As illustrated in Figure 4d, the currents of the anodic peak (I$_{pa}$) and cathodic peak (I$_{pc}$) maintained a good linear connection with the square root of the scanning speed, indicating that the oxidation of glucose on Mn$_3$O$_4$/NiO/CNFs/GCE is a diffusion-controlled process.

To improve the electrocatalytic effect of Mn$_3$O$_4$/NiO/CNFs on glucose detection, the time-current method was used to optimize the parameters during the experiments, including the applied voltage and the concentrations of NaOH and Mn$_3$O$_4$/NiO/CNFs. Figure 5a shows that the response current increases with increasing applied voltage at the beginning, and then decreases when the applied voltage is higher than 0.50 V. Thus, 0.50 V is the optimum applied potential. In Figure 5b, the response current initially increases with increasing concentration of NaOH, and then starts to decrease when the concentration of NaOH exceeds 0.10 M. Therefore, 0.1 M NaOH was chosen as the optimum concentration of electrolyte. Figure 5c shows that the response current reaches its maximum when the concentration of Mn$_3$O$_4$/NiO/CNFs is 9 mg mL^{-1}; therefore, 9 mg mL^{-1} was selected as the optimum modification material concentration. Figure 6a shows the current response of Mn$_3$O$_4$/NiO/CNFs/GCE for continuous addition of glucose under known optimal experimental conditions. The relationship between response current and glucose concentration shows linearly in the range of 5–3000 μM (R^2 = 0.997) and 3000–12,000 μM (R^2 = 0.993), and could be well-fitted to the equation: I (μA) = 27.33 C (mM) + 1.343 and I (μA) = 17.22 C (mM) + 35.015. The detection limit of Mn$_3$O$_4$/NiO/CNFs/GCE was calculated to be 0.73 μM (S/N = 3). The sensitivity was calculated to be 386.84 μA mM^{-1} cm^{-2} (5–3000 μM) and 243.74 μA mM^{-1} cm^{-2} (3000–12,000 μM). Additionally, the response time is a key factor in weighing up the practical application of the sensor. Figure S3 shows that the Mn$_3$O$_4$/NiO/CNFs/GCE at different glucose concentrations reaches its steady-state current within 2–4 s after the addition of glucose. Table 1 lists the electrocatalytic effects of some reported enzyme-free glucose sensors and enzymatic glucose sensors. Compared with them, our proposed Mn$_3$O$_4$/NiO/CNFs/GCE has a wider linear range as well as lower detection limit as glucose sensor.

Table 1. Performance comparison of the proposed Mn$_3$O$_4$/NiO/CNFs/GCE with other glucose sensors.

Sensing Material	Linear Range (μM)	Detection Limit (μM)	Sensitivity (μA mM^{-1} cm^{-2})	Ref.
Mn$_3$O$_4$@ZIF-67/CC [1]	0.8–6000	0.24	3421.0	[40]
CuCo$_2$O$_4$/NiO/CC	0.5–6000	0.28	4140	[14]
Cu$_2$O-Cu-Au	0–4500	1.71	1082	[41]
Cu-Ni/NF	1–600	2	11,340.25	[42]
NiMoO$_4$/CNF	0.3–4500	0.05	301.77	[43]
Ni$_2$P-Cu$_3$P	4–5000	0.1	4700	[44]
ZnO/MXene	50–700	17	29	[45]
Co$_{0.33}$Ni$_{0.67}$-HLDH [2]	10–2000	3.1	242.9	[46]
Mn$_3$O$_4$/NiO	9.9–3665	1.0	226.2	[47]
MnO$_2$/Co$_3$O$_4$	60–7000	0.03	127	[48]
FTO-CNTs/PEI/GOX	70–700	70	63.38	[49]
PEDOT: SCX/MXene/GOX/GCE	500–8000	22.5	-	[50]
Ni-MOF [3]/rGO [4]/CF [5]	6–2090	0.6	852	[51]
Mn$_3$O$_4$/NiO/CNFs	5–3000 3000–12,000	0.73	386.84 243.74	This work

[1] Carbon cloth. [2] Hollow layered double hydroxides. [3] Metal organic frameworks. [4] Reduced graphene oxide. [5] Carbon fiber.
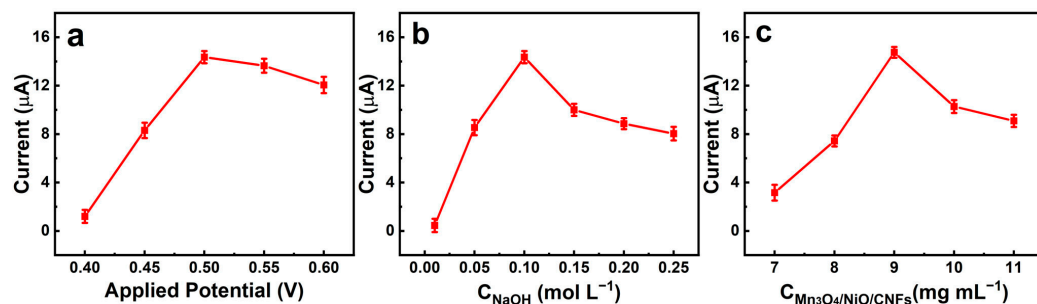
Figure 5. Optimization of parameters on the current response of 0.5 mM glucose: (**a**) applied potential; (**b**) the concentration of NaOH; (**c**) the content of $Mn_3O_4/NiO/CNFs$.
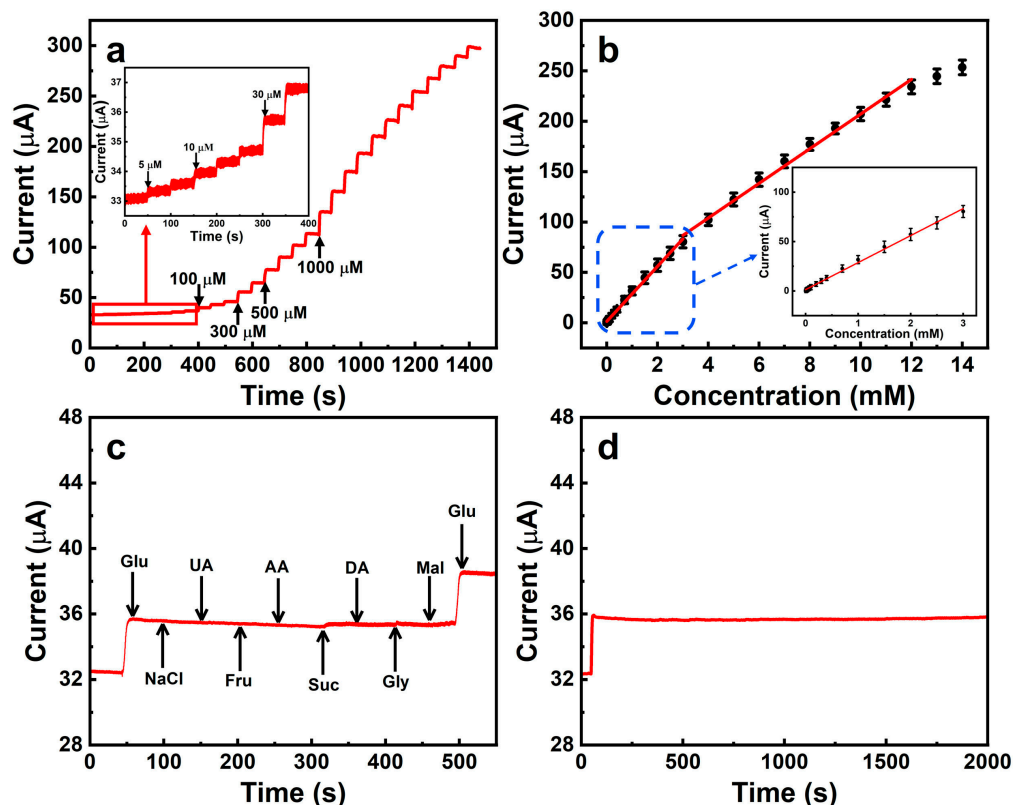

Figure 6. (**a**) Amperometric response of $Mn_3O_4/NiO/CNFs$ electrode for different concentrations of glucose (inset is current response at low concentrations); (**b**) calibration curves corresponding to (**a**); (**c**) current response of $Mn_3O_4/NiO/CNFs$ electrode to 100 μM glucose and different interferences; (**d**) the stability test of $Mn_3O_4/NiO/CNFs$ electrode during the 2000 s. All the above experiments were conducted under optimal parameters.

3.4. Selectivity, Stability, Repeatability, and Reproducibility of $Mn_3O_4/NiO/CNFs/GCE$

The presence of other easily oxidized molecules in the actual sample may affect the accuracy of glucose detection. In Figure 6c, the addition of 5 μM of some interferences to 100 μM glucose solution at the ratio of 1:20 was investigated by a time-current test. The outcomes showed that the current responses caused by the addition of interferences were virtually negligible, indicating that $Mn_3O_4/NiO/CNFs/GCE$ had good selectivity. Figure 6d shows the amperometric response of $Mn_3O_4/NiO/CNFs/GCE$ to 100 μM glucose. The current kept stable during 2000 s, suggesting that the electrode had an excellent stability as glucose sensor. Besides, repeatability and reproducibility are also key to determine whether the synthesized materials can be used for actual sample detection. The five identical modified electrodes used to detect 0.1 mM glucose were found to have a relative

standard deviation (RSD) of 6.38% (Figure S4), indicating that the electrodes have good reproducibility. The modified electrode was repeated five times to detect 0.1 mM glucose, and the RSD was calculated to be 1.32% (Figure S5), meaning that the electrode has a good repeatability. To evaluate the long-term stability of the sensor, the $Mn_3O_4/NiO/CNFs/GCE$ was stored at room temperature for 30 days. The results show that the response current remains at 95.3% of the initial current after 30 days (Figure S6), indicating that our sensors have satisfactory long-term stability.

3.5. Actual Sample Analysis

To evaluate the practicality of $Mn_3O_4/NiO/CNFs/GCE$, serum samples with different concentrations of glucose were detected using standard addition method. The serum samples used in the experiment were from the School of Medicine, Shanghai University. The recoveries of the three samples were 100.09%, 100.20%, and 99.91%, respectively (Table 2), indicating that the built sensor can be accepted for glucose detection in serum samples.

Table 2. Analysis of glucose in human blood serum.

Sample	Detected (mM)	Commercial Method (mM)	RSD (%)	Recovery (%)
1	4.72	4.59	1.91	100.09
2	4.83	4.69	1.47	100.2
3	8.00	7.67	2.34	99.91

4. Conclusions

In this work, $Mn_3O_4/NiO/CNFs$ were synthesized by electrospinning and following calcination, and were used as an enzyme-free sensor for glucose detection. The intricate network structure of CNFs provides the backbone for the nanoparticles and facilitates electron transport. In addition, the synergistic effect between Mn_3O_4 and NiO is beneficial to improve the catalytic performance for glucose detection. The constructed $Mn_3O_4/NiO/CNFs/GCE$ sensor has good linear range, low detection limit, and anti-interference ability, indicating that $Mn_3O_4/NiO/CNFs$ have some application prospects as electrochemical sensors in clinical diagnosis.

Author Contributions: Conceptualization, M.L. and S.L.; methodology, X.Y. and S.L.; software, J.D. and X.O.; validation, M.L., J.D. and X.O.; formal analysis, J.D., X.O., S.L. and X.Y.; investigation, M.L. and S.L.; resources, L.L. and D.D.; data curation, M.L., J.D. and X.O.; writing—original draft preparation, M.L.; writing—review and editing, L.L., D.D. and X.Y.; visualization, S.L. and X.Y.; supervision, D.D. and L.L.; project administration, D.D. and L.L.; funding acquisition, D.D. and L.L. All authors have read and agreed to the published version of the manuscript.

Institutional Review Board Statement: Not applicable.

Informed Consent Statement: Not applicable.

Data Availability Statement: Date will be made available on request.

References

1.   Wang, D.; Chang, Y. The Construct CoSe$_2$ on Carbon Nanosheets as High Sensitivity Catalysts for Electrocatalytic Oxidation of Glucose. *Nanomaterials* **2022**, *12*, 572. [CrossRef] [PubMed]
2.   Wang, S.; Li, S.P.; Wang, W.W.; Zhao, M.T.; Liu, J.F.; Feng, H.F.; Chen, Y.M.; Du, Y.; Hao, W.C. A Non-Enzymatic Photoelectro-chemical Glucose Sensor Based on BiVO$_4$ Electrode under Visible Light. *Sens. Actuators B* **2019**, *291*, 34–41. [CrossRef]
3.   Cao, F.H.; Zhou, Y.; Wu, J.; Li, W.; Zhang, C.L.; Ni, G.; Cui, P.; Song, C.J. Electrospinning One-dimensional Surface-phosphorized CuCo/C Nanofibers for Enzyme-free Glucose Sensing. *New J. Chem.* **2022**, *46*, 11531–11539. [CrossRef]
4.   Adeel, M.; Rahman, M.M.; Caligiuri, I.; Canzonieri, V.; Rizzolio, F.; Daniele, S. Recent Advances of Electrochemical and Optical Enzyme-Free Glucose Sensors Operating at Physiological Conditions. *Biosens. Bioelectron.* **2020**, *165*, 112331. [CrossRef]
5.   Liu, S.; Qiu, Y.Z.; Liu, Y.F.; Zhang, W.F.; Dai, Z.; Srivastava, D.; Kumar, A.; Pan, Y.; Liu, J.Q. Recent Advances in Bimetallic Metal-organic Frameworks (BMOFs): Synthesis, Applications and Challenges. *New J. Chem.* **2022**, *46*, 13818–13837. [CrossRef]
6.   Li, L.T.; Zou, J.F.; Han, Y.T.; Liao, Z.H.; Lu, P.F.; Nezamzadeh-Ejhieh, A.; Liu, J.Q.; Peng, Q.P. Recent Advances in Al(iii)/In(iii)-based MOFs for the Detection of Pollutants. *New J. Chem.* **2022**, *46*, 19577–19592. [CrossRef]
7.   Gao, H.; Xiao, F.; Ching, C.B.; Duan, H. One-Step Electrochemical Synthesis of PtNi Nanoparticle-Graphene Nanocomposites for Nonenzymatic Amperometric Glucose Detection. *ACS Appl. Mater. Interfaces* **2011**, *3*, 3049–3057. [CrossRef]
8.   Li, Y.Y.; Tang, L.; Deng, D.M.; He, H.B.; Yan, X.X.; Wang, J.H.; Luo, L.Q. Hetero-Structured MnO-Mn$_3$O$_4$@rGO Composites: Synthesis and Nonenzymatic Detection of H$_2$O$_2$. *Mater. Sci. Eng. C* **2021**, *118*, 111443. [CrossRef]
9.   Liu, X.Z.; Yang, H.P.; Diao, Y.Y.; He, Q.; Lu, C.Y.; Singh, A.; Kumar, A.; Liu, J.Q.; Lan, Q. Recent Advances in the Electrochemical Applications of Ni-based Metal Organic Frameworks (Ni-MOFs) and Their Derivatives. *Chemosphere* **2022**, *307*, 135729. [CrossRef]
10. Saxena, A.; Liyanage, W.P.R.; Kapila, S.; Nath, M. Nickel Selenide as an Efficient Electrocatalyst for Selective Reduction of Carbon Dioxide to Carbon-rich Products. *Catal. Sci. Technol.* **2022**, *12*, 4727–4739. [CrossRef]
11. Li, M.R.; Zheng, K.T.; Zhang, J.J.; Li, X.M.; Xu, C.J. Design and Construction of 2D/2D Sheet-on-sheet Transition Metal Sulfide/Phosphide Heterostructure for Efficient Oxygen Evolution Reaction. *Appl. Surf. Sci.* **2021**, *565*, 150510. [CrossRef]
12. Sivanantham, A.; Shanmugam, S. Graphitic Carbon-NiCo Nanostructures as Efficient Non-precious-metal Electrocatalysts for the Oxygen Reduction Reaction. *ChemElectroChem* **2018**, *5*, 1937–1943. [CrossRef]
13. Hernandez-Ramirez, D.; Mendoza-Huizar, L.H.; Galan-Vidal, C.A.; Aguilar-Lira, G.Y.; Alvarez-Romero, G.A. Development of a Non-Enzymatic Glucose Sensor Based on Fe$_2$O$_3$ Nanoparticles-carbonve and Analytica Paste Electrodes. *J. Electrochem. Soc.* **2022**, *169*, 067507. [CrossRef]
14. Wang, H.; Li, Y.Y.; Deng, D.M.; Li, M.J.; Zhang, C.Y.; Luo, L.Q. NiO-Coated CuCo$_2$O$_4$ Nanoneedle Arrays on Carbon Cloth for Nonenzymatic Glucose Sensing. *ACS Appl. Nano Mater.* **2021**, *4*, 9821–9830. [CrossRef]
15. Xu, Y.H.; Ding, Y.P.; Zhang, L.H.; Zhang, X.X. Highly Sensitive Enzyme-free Glucose Sensor Based on CuO-NiO Nanocomposites by Electrospinning. *Compos. Commun.* **2021**, *25*, 100687. [CrossRef]
16. Zhang, R.; Zhou, T.T.; Zhang, T. Functionalization of Hybrid 1D SnO$_2$-ZnO Nanofibers for Formaldehyde Detection. *Adv. Mater. Interfaces* **2018**, *5*, 1800967. [CrossRef]
17. Thomas, T.; Jayababu, N.; Shruthi, J.; Mathew, A.; Cerdan-Pasaran, A.; Hernandez-Magallanes, J.A.; Sanal, K.C.; Reshmi, R. Room Temperature Ammonia Sensing of Alpha-MoO$_3$ Nanorods Grown on Glass Substrates. *Thin Solid Films* **2021**, *722*, 138575. [CrossRef]
18. Zhang, C.Y.; Li, Y.Y.; Wang, H.; Niu, X.Y.; Deng, D.M.; Qin, X.; Yan, X.X.; He, H.B.; Luo, L.Q. Low Temperature Growth of CuS Nanosheets on Hollow Co$_9$S$_8$ Nanotubes: Synthesis and Analytical Application. *Microchem. J.* **2022**, *183*, 108037. [CrossRef]
19. Kokulnathan, T.; Vishnuraj, R.; Chen, S.M.; Pullithadathil, B.; Ahmed, F.; Hasan, P.M.Z.; Bilgrami, A.L.; Kumar, S. Tailored Construction of One-Dimensional TiO$_2$/Au Nanofibers: Validation of an Analytical Assay for Detection of Diphenylamine in Food Samples. *Food Chem.* **2022**, *380*, 132052. [CrossRef] [PubMed]
20. Wang, C.H.; Kim, J.; Kim, M.; Lim, H.; Zhang, M.; You, J.; Yun, J.H.; Bando, Y.; Li, J.S.; Yamauchi, Y. Nanoarchitectured Metal-Organic Framework-Derived Hollow Carbon Nanofiber Filters for Advanced Oxidation Processes. *J. Mater. Chem. A* **2019**, *7*, 13743–13750. [CrossRef]
21. Zhang, Z.X.; Wang, Y.X.; Leng, X.X.; Crespi, V.H.; Kang, F.Y.; Lv, R.T. Controllable Edge Exposure of MoS$_2$ for Efficient Hydrogen Evolution with High Current Density. *ACS Appl. Energy Mater.* **2018**, *1*, 1268–1275. [CrossRef]
22. Sui, L.L.; Yu, T.T.; Zhao, D.; Cheng, X.L.; Zhang, X.F.; Wang, P.; Xu, Y.M.; Gao, S.; Zhao, H.; Gao, Y.; et al. In Situ Deposited Hierarchical CuO/NiO Nanowall Arrays Film Sensor with Enhanced Gas Sensing Performance to H$_2$S. *J. Hazard. Mater.* **2020**, *385*, 121570. [CrossRef]
23. Liu, S.Y.; Xie, J.; Zheng, Y.X.; Cao, G.S.; Zhu, T.J.; Zhao, X.B. Nanocrystal Manganese Oxide (Mn$_3$O$_4$, MnO) Anchored on Graphite Nanosheet with Improved Electrochemical Li-Storage Properties. *Electrochim. Acta* **2012**, *66*, 271–278. [CrossRef]
24. Niu, H.T.; Zhang, J.; Xie, Z.L.; Wang, X.G.; Lin, T. Preparation, Structure and Supercapacitance of Bonded Carbon Nanofiber Electrode Materials. *Carbon* **2011**, *49*, 2380–2388. [CrossRef]
25. Abe, J.; Takahashi, K.; Kawase, K.; Kobayashi, Y.; Shiratori, S. Self-Standing Carbon Nanofiber and SnO$_2$ Nanorod Composite as a High-Capacity and High-Rate-Capability Anode for Lithium-Ion Batteries. *ACS Appl. Nano Mater.* **2018**, *1*, 2982–2989. [CrossRef]

26. Yang, G.; Li, Y.H.; Ji, H.M.; Wang, H.Y.; Gao, P.; Wang, L.; Liu, H.D.; Pinto, J.; Jiang, X.F. Influence of Mn Content on the Morphology and Improved Electrochemical Properties of Mn_3O_4 Vertical Bar MnO@Carbon Nanofiber as Anode Material for Lithium Batteries. *J. Power Source* **2012**, *216*, 353–362. [CrossRef]

27. Rani, B.J.; Rathika, S.; Ravi, G.; Yuvakkumar, R. Synthesis of $MnNiO_3/Mn_3O_4$ Nanocomposites for the Water Electrolysis Process. *J. Sol-Gel Sci. Technol.* **2019**, *92*, 1–11. [CrossRef]

28. Liu, M.M.; An, M.L.; Xu, J.Q.; Liu, T.; Wang, L.L.; Liu, Y.Y.; Zhang, J.J. Three-Dimensional Carbon Foam Supported NiO Nanosheets as Non-Enzymatic Electrochemical H_2O_2 sensors. *Appl. Surf. Sci.* **2021**, *542*, 148699. [CrossRef]

29. Pan, J.Q.; Li, S.; Ou, W.; Liu, Y.Y.; Li, H.L.; Wang, J.J.; Song, C.S.; Zheng, Y.Y.; Li, C.R. The Photovoltaic Conversion Enhancement of $NiO/Tm:CeO_2/SnO_2$ Transparent P-N Junction Device with Dual-Functional $Tm:CeO_2$ Quantum Dots. *Chem. Eng. J.* **2020**, *393*, 124802. [CrossRef]

30. Zhang, Y.Q.; Wang, Y.Z.; Jia, J.B.; Wang, J.G. Nonenzymatic Glucose Sensor Based on Graphene Oxide and Electrospun NiO Nanofibers. *Sens. Actuators B* **2012**, *171*, 580–587. [CrossRef]

31. Alegre, C.; Busacca, C.; Di Blasi, A.; Di Blasi, O.; Arico, A.S.; Antonucci, V.; Modica, E.; Baglio, V. Electrospun Carbon Nanofibers Loaded with Spinel-Type Cobalt Oxide as Bifunctional Catalysts for Enhanced Oxygen Electrocatalysis. *J. Energy Storage* **2019**, *23*, 269–277. [CrossRef]

32. Busacca, C.; Di Blasi, O.; Giacoppo, G.; Briguglio, N.; Antonucci, V.; Di Blasi, A. High Performance Electrospun Nickel Manganite on Carbon Nanofibers Electrode for Vanadium Redox Flow Battery. *Electrochim. Acta* **2020**, *355*, 136755. [CrossRef]

33. Huan, K.; Li, Y.Y.; Deng, D.M.; Wang, H.; Wang, D.J.; Li, M.J.; Luo, L.Q. Composite-Controlled Electrospinning of CuSn Bimetallic Nanoparticles/Carbon Nanofibers for Electrochemical Glucose Sensor. *Appl. Surf. Sci.* **2022**, *573*, 151528. [CrossRef]

34. Hao, Z.Y.; Meng, Z.S.; Li, X.Y.; Sun, X.C.; Xu, J.; Nan, H.; Shi, W.; Qi, G.J.; Hu, X.Y.; Tian, H.W. Two-Step Fabrication of Lanthanum Nickelate and Nickel Oxide Core-Shell Dandelion-Like Materials for High-Performance Supercapacitors. *J. Colloid Interface Sci.* **2022**, *617*, 430–441. [CrossRef] [PubMed]

35. Zhang, W.J.; Guo, X.L.; Zhao, J.J.; Zheng, Y.M.; Xie, H.; Zhang, Z.; Wang, S.H.; Xu, Q.; Fu, Q.P.; Zhang, T. High Performance Flower-Like Mn_3O_4/rGO Composite for Supercapacitor Applications. *J. Electroanal. Chem.* **2022**, *910*, 116170. [CrossRef]

36. Singer, N.; Pillai, R.G.; Johnson, A.I.D.; Harris, K.D.; Jemere, A.B. Nanostructured Nickel Oxide Electrodes for Non-Enzymatic Electrochemical Glucose Sensing. *Microchim. Acta* **2020**, *187*, 196. [CrossRef]

37. Dong, C.J.; Tao, Y.; Chang, Q.; Liu, Q.H.; Guan, H.T.; Chen, G.; Wang, Y.D. Direct Growth of $MnCO_3$ on Ni Foil for a Highly Sensitive Nonenzymatic Glucose Sensor. *J. Alloys Compd.* **2018**, *762*, 216–221. [CrossRef]

38. Zhang, Y.Y.; Huang, Y.Q.; Gao, P.P.; Yin, W.; Yin, M.; Pu, H.C.; Sun, Q.Q.; Liang, X.L.; Huan, B.H. Bimetal-organic Frameworks MnCo-MOF-74 Derived Co/MnO@HC for the Construction of a Novel Enzyme-free Glucose sensor. *Microchem. J.* **2022**, *175*, 107097. [CrossRef]

39. Wang, L.J.; Li, Y.Y.; Zhang, C.Y.; Deng, D.M.; He, H.B.; Yan, X.X.; Li, Z.G.; Luo, L.Q. Hierarchical NiMn Layered Double Hydroxide Nanostructures on Carbon Cloth for Electrochemical Detection of Hydrogen Peroxide. *ACS Appl. Nano Mater.* **2022**, *5*, 17741–17749. [CrossRef]

40. Dong, Q.Y.; He, Z.Y.; Tang, X.; Zhang, Y.; Yang, L.; Huang, K.; Jiang, X.; Xiong, X.L. One-Step Synthesis of Mn_3O_4@ZIF-67 on Carbon Cloth: As an Effective Non-Enzymatic Glucose Sensor. *Microchem. J.* **2022**, *175*, 107203. [CrossRef]

41. Pu, F.Z.; Miao, H.R.; Lu, W.J.; Zhang, X.J.; Yang, Z.M.; Kong, C.C. High-Performance Non-Enzymatic Glucose Sensor Based on Flower-Like Cu_2O-Cu-Au Ternary Nanocomposites. *Appl. Surf. Sci.* **2022**, *581*, 152389. [CrossRef]

42. Wei, H.G.; Xu, Q.Z.; Li, A.; Wan, T.; Huang, Y.; Cui, D.P.; Pan, D.; Dong, D.D.; Wei, R.B.; Naik, N.; et al. Dendritic Core-Shell Copper-Nickel Alloy@Metal Oxide for Efficient Non-Enzymatic Glucose Detection. *Sens. Actuators B* **2021**, *337*, 129687. [CrossRef]

43. Rani, S.D.; Ramachandran, R.; Sheet, S.; Aziz, M.A.; Lee, Y.S.; Al-Sehemi, A.G.; Pannipara, M.; Xia, Y.; Tsai, S.Y.; Ng, F.L.; et al. $NiMoO_4$ Nanoparticles Decorated Carbon Nanofiber Membranes for the Flexible and High Performance Glucose Sensors. *Sens. Actuators B* **2020**, *312*, 127886. [CrossRef]

44. He, L.; Li, J.W.; Cao, J.; Li, X.; Feng, X.F.; Zhang, J.; Yang, Y. High Performance of Non-Enzymatic Glucose Biosensors Based on the Design of Microstructure of Ni_2P/Cu_3P Nanocomposites. *Appl. Surf. Sci.* **2022**, *593*, 153395. [CrossRef]

45. Myndrul, V.; Coy, E.; Babayevska, N.; Zahorodna, V.; Balitskyi, V.; Baginskiy, I.; Gogotsi, O.; Bechelany, M.; Giardi, M.T.; Iatsunskyi, I. MXene Nanoflakes Decorating ZnO Tetrapods for Enhanced Performance of Skin-Attachable Stretchable Enzymatic Electrochemical Glucose Sensor. *Biosens. Bioelectron.* **2022**, *207*, 114141. [CrossRef]

46. Kong, X.Y.; Xia, B.; Xiao, Y.W.; Chen, H.H.; Li, H.F.; Chen, W.Z.; Wu, P.; Shen, Y.; Wu, J.S.; Li, S.; et al. Regulation of Cobalt-Nickel LDHs' Structure and Components for Optimizing the Performance of an Electrochemical Sensor. *ACS Appl. Nano Mater.* **2019**, *2*, 6387–6396. [CrossRef]

47. Wang, Y.; Cui, J.W.; Wang, Y.; Yu, D.B.; Cheng, S.; Zheng, H.M.; Shu, X.; Zhang, Y.; Wu, Y.C. Decorating Mn_3O_4 Nanoparticle on NiO Nanoflake Arrays for High-performance Electrochemical Biosensors. *J. Solid State Electrochem.* **2019**, *23*, 135–142. [CrossRef]

48. Sinha, L.; Pakhira, S.; Bhojane, P.; Mali, S.; Hong, C.K.; Shirage, P.M. Hybridization of Co_3O_4 and alpha-MnO_2 Nanostructures for High-Performance Nonenzymatic Glucose Sensing. *ACS Sustain. Chem. Eng.* **2018**, *6*, 13248–13261. [CrossRef]

49. Tai, N.H.; Lin, M.H.; Gupta, S.; Chang, C.; Lee, C.Y. Carbon Nanotubes/Polyethylenimine/Glucose Oxidase as a Non-invasive Electrochemical Biosensor Performs High Sensitivity for Detecting Glucose in Saliva. *Microchem. J.* **2022**, *180*, 107547. [CrossRef]

50. Murugan, P.; Annamalai, J.; Atchudan, R.; Govindasamy, M.; Nallaswamy, D.; Ganapathy, D.; Reshetilov, A.; Sundramoorthy, A.K. Electrochemical Sensing of Glucose Using Glucose Oxidase/PEDOT:4-Sulfocalix 4 arene/MXene Composite Modified Electrode. *Micromachines* **2022**, *13*, 304. [CrossRef]

51. Dong, S.; Niu, H.W.; Sun, L.W.; Zhang, S.X.; Wu, D.Q.; Yang, Z.; Xiang, M. Highly Dense Ni-MOF Nanoflake Arrays Supported on Conductive Graphene/Carbon Fiber Substrate as Flexible Microelectrode for Electrochemical Sensing of Glucose. *J. Electroanal. Chem.* **2022**, *911*, 116219. [CrossRef]